Chemical Raman Enhancement of Organic Adsorbates on Metal Surfaces

A. T. Zayak,[1,2] Y. S. Hu,[3] H. Choo,[1,2] J. Bokor,[1,2] S. Cabrini,[1] P. J. Schuck,[1] and J. B. Neaton[1,*]

[1]*Molecular Foundry, Lawrence Berkeley National Laboratory, Berkeley California 94720, USA*
[2]*Department of Electrical Engineering and Computer Sciences, UC Berkeley, Berkeley California 94720-1770, USA*
[3]*Bioengineering Department, Rice University, Houston, Texas 77005, USA*

Using first-principles theory and experiments, chemical contributions to surface-enhanced Raman spectroscopy for a well-studied organic molecule, benzene thiol, chemisorbed on planar Au(111) surfaces are explained and quantified. Density functional theory calculations of the static Raman tensor demonstrate a strong mode-dependent modification of benzene thiol Raman spectra by Au substrates. Raman active modes with the largest enhancements result from stronger contributions from Au to their electron-vibron coupling, as quantified through a deformation potential. A straightforward and general analysis is introduced to extract chemical enhancement from experiments for specific vibrational modes; measured values are in excellent agreement with our calculations.

Since its discovery over three decades ago, surface-enhanced Raman spectroscopy (SERS) has shown significant promise for sensing individual molecules adsorbed near metal nanostructures or substrates with nanoscale roughness [1–3]. In SERS, the conversion of incident light into surface plasmons near nanoscale asperities on metal surfaces, combined with chemical and resonant effects, has been reported to yield Raman cross sections increased by factors of up to 10^{14}, enabling single-molecule detection [4–9]. While the enhancement associated with surface plasmons can reach 10^8 [10], remaining increases and associated changes in mode frequencies have been reported to arise from chemical adsorption [4,11–16], as well as resonant intramolecular and metal-molecule charge transfer [17–19]. Despite a wealth of prior theoretical studies, these chemical enhancement (CE) mechanisms are poorly understood and difficult to quantify [4,12–14]. While for some vibrational modes CE is estimated [4,11,12,20] to be about 10–100, there is currently no clear picture for why certain modes are enhanced more than others. Previous theoretical studies have proposed mechanisms for this mode dependence [14–19], but none of these models have been validated by experiments or more rigorous first-principles calculations, leaving the origin of dominant chemical contributions to SERS an open question [4,12–14].

In this Letter, we use first-principles calculations and experiment to explain chemical contributions to SERS for (C_6H_5SH) benzene thiol (BT) molecule chemisorbed to Au surfaces. From our density functional theory (DFT) calculations of static contributions to the Raman tensor, we elucidate the vibrational mode dependence [4,12–14] of the chemical enhancement, explicitly relating modes with the largest CE to those with the greatest mode-induced shift of the molecular frontier orbital energy, as quantified through a deformation potential. Relative CE of BT vibra-

tional modes measured at different probe frequencies agree quantitatively with our static calculations for all binding sites considered. While the magnitude of CE for BT on Au is sensitive to binding motif, its relative value is not.

DFT calculations are performed using the Vienna *ab initio* simulation package (VASP) and within a generalized gradient approximation [21,22]. We model the BT adsorbate-Au substrate system with an ordered monolayer of about one BT molecule per nm^2 bonded to a flat periodic Au(111) slab. A 400 eV plane-wave cutoff and $2 \times 2 \times 1$ Monkhorst-Pack k-point mesh is used for calculations involving Au slabs. Four binding geometries are considered, as shown in Fig. 1(b): fcc hollow ($E_B = 0.219$ eV), adatom ($E_B = 0.446$ eV), hydrogenated adatom ($E_B = 0.795$ eV), and bridge ($E_B = 0.192$ eV), where E_B is the calculated binding energy relative to a free Au surface and gas-phase C_6H_5SH in the dilute limit. The gas-phase BT molecule is simulated in the same large supercell as the slab geometry, using the Γ point.

Static Raman tensors are constructed mode-by-mode using a finite-differences approach, in two steps. First, the dynamical matrix of the system is generated by displacing each atom along each Cartesian direction by 0.03 Å. Vibrational frequencies and corresponding phonon eigenvectors are obtained by diagonalization of a truncated dynamical matrix treating only BT atoms, and Au atoms directly bonded with sulfur. Second, we compute the static polarizability from a second-order finite-difference expression using a sawtooth potential with a gradient of 1 mV/Å, and compute its derivative as a function of the amplitude for each vibrational eigenmode. (See supplemental material for additional details [23].) Throughout the Letter, all modes are labeled with gas-phase frequencies for simplicity.

In Fig. 1(a), we report Raman cross sections calculated from the dominant (nonevanescent) component of the
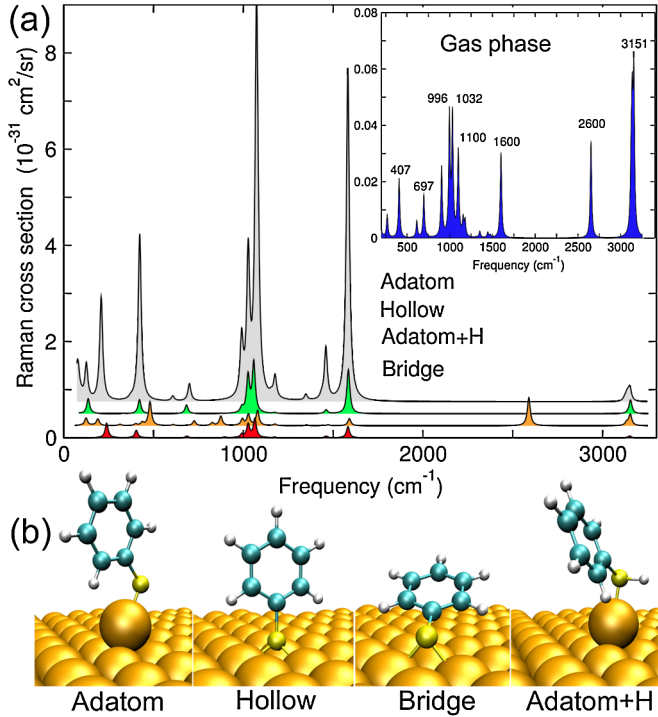
FIG. 1 (color online). (A) Calculated Raman spectra of BT (from R_{zz} components only) for four different binding geometries: adatom, hollow, adatom + H, and bridge. Inset shows our calculations of the orientationally-averaged gas-phase Raman spectrum of benzene thiol. All spectra are broadened with a Lorentzian of 10 cm^{-1} width. (B) Binding geometries. Our supercell consists of 5 atomic layers of Au stacked along [111] with 16 atoms per layer, with 30 Å of vacuum. The in-plane lattice parameters are kept fixed to their computed Au fcc bulk value of 4.17 Å.

Raman tensor, R_{zz}, where z is the normal to the surface. Prominent Raman peaks in the computed spectra agree well with experiment [24]. Upon adsorption, BT vibrational frequencies are altered on average by 10–20 cm^{-1}, in agreement with experiments (see [23]). From Fig. 1(a), the presence of the Au substrate enhances Raman cross sections for some modes more than for others. The intensities of modes with larger enhancements exhibit a stronger dependence on binding site. For example, while the intensity of the 1100 cm^{-1} mode varies by more than 2 orders of magnitude across the different sites considered, the intensity of the 3151 cm^{-1} mode remains relatively unaltered and comparable to the gas-phase intensity.

In Fig. 2(a), we compare the computed charge density change induced by these two modes, $\delta\rho(Q_n) = \rho(Q_n) - \rho(0)$, where Q_n is the vibrational eigenvector amplitude. We find that the 1100 cm^{-1} mode induces significant charge redistribution within the Au surface, while the 3151 cm^{-1} mode does not. This behavior is entirely consistent with mode-induced changes observed in the DFT electronic structure [Fig. 2(b)]: The peak Kohn-Sham HOMO energy E_{HOMO} shifts noticeably relative to the Fermi level E_F with the 1100 cm^{-1} mode, whereas the
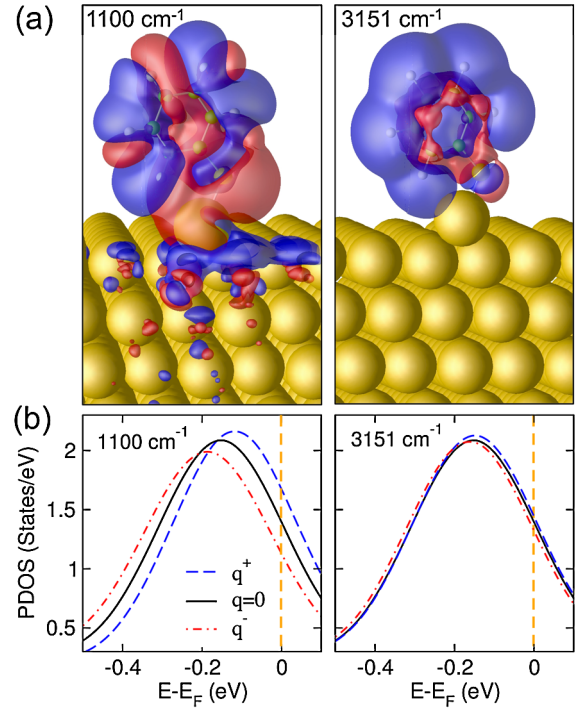

FIG. 2 (color online). (A) Computed isosurfaces (at $1.65 \times 10^{-4}\ e/\text{Å}^3$) of charge density induced by freezing-in small amplitudes (0.1 Å) of the 1100 and 3151 cm^{-1} modes. For both modes, gold atoms are stationary, and charge rearrangement in the substrate is induced by the molecule. (B) Partial densities of states projected on the molecule near the Au Fermi energy for three different amplitudes.

3151 cm^{-1} mode leaves the HOMO peak unchanged. Examining all modes, we find that modes that show larger enhancements induce a larger polarization response in the substrate (and larger shift in E_F-E_{HOMO}).

To rationalize our DFT results, we compare a model expression for the static polarizability and Raman tensor with our more rigorous first-principles calculations. We consider a single (dominant) term in an approximate single-particle form for the ground state electronic polarizability α, one that includes just a lone virtual transition between the HOMO, φ_{HOMO}, and a metallic state at E_F, ϕ_{Au}. Within this two-state approximation, an adsorbate-metal interfacial contribution to the Raman tensor $R_{\mathrm{BT\text{-}Au}}$ can be expressed as [13,14]

$$R_{\mathrm{BT\text{-}Au}} = \frac{\partial \alpha_{\mathrm{BT\text{-}Au}}}{\partial Q_n} \approx \frac{1}{\omega_{\mathrm{H}}} \frac{\partial M_i^* M_j}{\partial Q_n} - \frac{M_i^* M_j}{\omega_{\mathrm{H}}^2} \frac{\partial \omega_{\mathrm{H}}}{\partial Q_n} \quad (1)$$

where $M_i = \langle \varphi_{\mathrm{HOMO}} \mid \mu_i \mid \phi_{\mathrm{Au}} \rangle$ is a dipole matrix element in the Cartesian direction i, and $\omega_{\mathrm{H}} = E_F$-$E_{\mathrm{HOMO}}$ is the difference between their eigenvalues. For modes that are not also IR active, terms involving derivatives of induced dipole moments can be neglected, and Eq. (1) reduces to a term proportional to $-\frac{1}{\omega_{\mathrm{H}}^2} \frac{\partial \omega_{\mathrm{H}}}{\partial Q_n}$. As noted previously[13,14], the ω_{H}^2 factor in the denominator is consistent with a sensitivity of the overall spectral

enhancement to the alignment of the frontier molecular electronic orbital with E_F. Indeed, this factor can be used to rationalize the binding site dependence of enhancements shown in Fig. 1(a), and corresponding partial densities of states shown on Fig. 3(a). Calculated enhancements on the adatom site, for which the HOMO is close to E_F, are significantly stronger than on other sites, where this level is broadened and further away from E_F. However, this ω_H^2 factor is the same for all modes, and cannot explain the mode-dependence of CE seen in Fig. 1(a).

The strong modification of the BT Raman spectra by the Au substrate can be explained via computation of a deformation potential, $\partial\omega_H/\partial Q_n$, for each mode, i.e., the change in molecular electronic level alignment, relative to E_F, induced by a particular vibration mode. In Fig. 3(b), we plot the difference $R_{zz}^{\text{Adatom}} - R_{zz}^{\text{Adatom+H}}$ against $\partial\omega_H/\partial Q_n$. Because the Kohn-Sham HOMO level of the adatom + H geometry is much further from E_F than for the adatom binding site [see Fig. 3(a)], ω_H is large, and the adatom + H geometry has a negligible interfacial contribution. Thus, to an excellent approximation, the difference $R_{zz}^{\text{Adatom}} - R_{zz}^{\text{Adatom+H}}$ removes intramolecular contributions to the Raman tensor unrelated to Eq. (1). Indeed, in Fig. 3(b), we find a remarkable correlation between the interface contribution to the deformation potential and enhancement for most of the vibrational modes. The modes that deviate from the linear trend at 407 cm^{-1} (Au-S stretch), 1475 cm^{-1} (phenyl ring stretch), and 3151 cm^{-1} (C-H stretch) have significant IR activity.

In the static limit used here, polarization induced by these IR-active modes screens the electric field experienced by the molecule, leading to a reduction in their Raman cross sections [25] by a factor proportional to $(Z_n^*)^2/\omega_n^2$, with the mode dynamical charge given by $Z_n^* = \Delta\mu/\Delta Q_n$ and where $\Delta\mu$ is the mode-induced interfacial dipole moment. In Fig. 3(c), we show the deviation δ of the IR-active "outlier" modes from the linear trend observed for non-IR-active modes versus $(Z_n^*)^2/\omega_n^2$. The correlation between δ and $(Z_n^*)^2/\omega_n^2$ confirms that modes with larger contributions to the screening lead to greater deviations from the two-state model [Fig. 3(b)]. We note however, that although important in our static calculations, this screening effect will have impact only below infrared frequencies, and thus will be inconsequential for typical probe frequencies, where the local fields will vary too rapidly for the IR-active vibrations to respond.

With this information, we can now connect the strong modification of Raman spectra by substrates to mode-specific changes of the electronic structure of the metal-adsorbate interface: modes with the largest interfacial contribution to the change in polarizability, as quantified through a deformation potential, result in the most substantial chemical enhancements. For BT, these modes are those that break the conjugation of the HOMO (supplemental material [23]). Figure 2(a) shows vividly how the 1100 cm^{-1} mode breaks the resonant character of the carbon ring, while the 3151 cm^{-1} mode leaves the π symmetry of the electrons on the phenyl ring intact. This suggests that for future adsorbates, the nature of modes with the largest CE might be intuitively rationalized *a priori*.

To validate our theory of chemical enhancement, we compare with experimental Raman and SERS
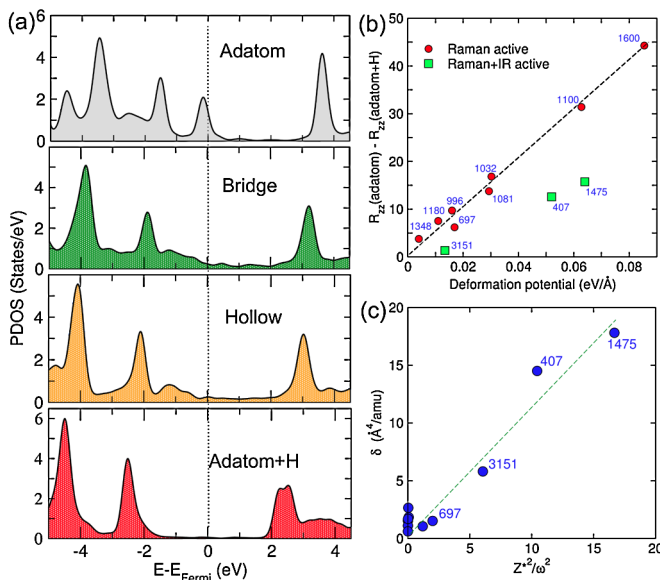
FIG. 3 (color online). (a) Partial densities of states projected on the molecule for different binding sites shown about the Au Fermi energy. (b) Difference $R_{zz}^{\text{Adatom}} - R_{zz}^{\text{Adatom+H}}$ plotted versus $\partial\omega_H/\partial Q_n$. (c) The deviation δ of these modes from linear trend in (b) plotted versus their contribution to the lattice susceptibility, which is proportional to the square of the ratio of the mode dynamical charge and its frequency.
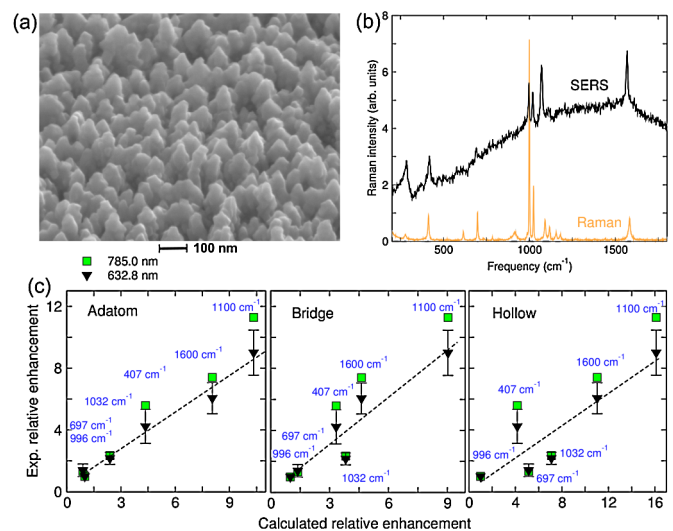
FIG. 4 (color online). (a) Au SERS substrate used in our measurements with BT. (b) Raman and SERS BT spectra. (c) Calculated relative enhancements versus experimental relative enhancements for adatom, bridge, and hollow sites.

measurements of BT on rough Au substrates [Figs. 4(a) and 4(b)]. SERS substrates, consisting of roughened SiGe surfaces [Fig. 4(a)] coated with 30 nm of Au, were incubated in 3 mM BT solution (Sigma Aldrich W361607) in methanol overnight, then gently rinsed with methanol and dried by nitrogen gas. Raman (neat solution) and SERS spectra were collected at two wavelengths, 632.8 nm and 785 nm, using an inverted microscope setup coupled to a spectrometer (Acton SpectraPro 2300i) equipped with a liquid-nitrogen-cooled charge-coupled device camera. To eliminate uncertainties associated with the number of molecular analytes in comparing Raman and SERS intensities, we normalize ratios of Raman and SERS spectra peak heights to the 996 cm^{-1} mode, which has only a modest enhancement from our calculations. We note that absolute CEs can be obtained if we normalize to a mode with zero deformation potential, $\partial \omega_H / \partial Q_n$, e.g., mode 1348 cm^{-1} in Fig. 3(b). As the 1348 cm^{-1} mode is not easily observed experimentally, we use 996 cm^{-1} in this case. Assuming the electromagnetic enhancement is the same for all modes, this relative enhancement will reflect CE. This assumption is acceptable for modes within a few hundred wave numbers of the 996 cm^{-1} mode, based on the width on relatively low Q factor for localized plasmon resonance in Au or Ag. In a more general case, the electromagnetic enhancement is not the same for all vibrational modes, and a plasmon resonance dispersion correction needs to be applied [26]. Additionally, in order to compare data from different experimental setups or different excitation wavelengths, spectral responses of specific experimental setups must be taken accounted for (see [23]).

In Fig. 4(c), we compare Raman cross sections from Fig. 1(a) (computed from R_{zz}) to averaged solution phase data from Fig. 1(a) (inset). Binding geometries for BT on flat Au surfaces are the subject of debate in the literature; and for rough surfaces at room temperature, a variety of adsorption sites will be available, and subject to thermal fluctuations [9,27]. By comparing three very different optimized binding sites to the experiment, we sample different possibilities for time-averaged experimental binding morphologies. Surprisingly, all three geometries show good correlation, with the adatom site perhaps showing the most linear trend. (We note that SERS measurements do not observe the S-H stretching mode at 2600 cm^{-1} indicating the loss of hydrogen at the S-Au in the room-temperature experiments.) Importantly, the relative theoretical enhancements, also normalized to the 996 cm^{-1} mode, are in excellent quantitative agreement with the present experiments, as well as others in literature taken from different substrates [28,29] (supplementary material), indicating standard DFT approaches can capture accurately and quantitatively dominant contributions to CE, even in the static limit. The quantitative agreement between theory and experiment, and the connection between deformation potential and chemical enhancement, provides new opportunities for detection and control of adsorbate-metal interactions through SERS.

*jbneaton@lbl.gov

[1] M. Fleischman, P. J. Hendra, and A. McQuillan, Chem. Phys. Lett. **26**, 163 (1974).
[2] D. L. Jeanmaire and R. P. V. Duyne, J. Electroanal. Chem. **84**, 1 (1977).
[3] M. G. Albrecht and J. A. Creighton, J. Am. Chem. Soc. **99**, 5215 (1977).
[4] M. Moskovits, J. Raman Spectrosc. **36**, 485 (2005).
[5] K. Kneipp et al., Phys. Rev. Lett. **78**, 1667 (1997).
[6] A. M. Michaels, J. Jiang, and L. Brus, J. Chem. Phys. **104**, 11 965 (2000).
[7] S. Nie and S. R. Emory, Science **275**, 1102 (1997).
[8] G. Haran, Acc. Chem. Res. **43**, 1135 (2010).
[9] D. R. Ward et al., Nano Lett. **8**, 919 (2008).
[10] K. A. Willets and R. P. V. Duyne, Annu. Rev. Phys. Chem. **58**, 267 (2007).
[11] M. Moskovits, Rev. Mod. Phys. **57**, 783 (1985).
[12] A. Campion and P. Kambhampati, Chem. Soc. Rev. **27**, 241 (1998).
[13] L. Jensen, C. M. Aikens, and G. C. Schatz, Chem. Soc. Rev. **37**, 1061 (2008).
[14] S. M. Morton and L. Jensen, J. Am. Chem. Soc. **131**, 4090 (2009).
[15] E. J. Heller, R. L. Sundberg, and D. Tannor, J. Phys. Chem. **86**, 1822 (1982).
[16] B. N. J. Persson, Chem. Phys. Lett. **82**, 561 (1981).
[17] F. J. Adrian, J. Chem. Phys. **77**, 5302 (1982).
[18] J. F. Arenas et al., J. Phys. Chem. **100**, 9254 (1996).
[19] J. R. Lombardi and R. L. Birke, J. Phys. Chem. C **112**, 5605 (2008).
[20] M. M. Maitani et al., J. Am. Chem. Soc. **131**, 6310 (2009).
[21] J. P. Perdew, K. Burke, and M. Ernzerhof, Phys. Rev. Lett. **77**, 3865 (1996).
[22] G. Kresse and J. Furthmüller, Phys. Rev. B **54**, 11 169 (1996).
[23] See supplemental material at http://link.aps.org/supplemental/10.1103/PhysRevLett.106.083003.
[24] V. Guieu et al., Opt. Express **17**, 24030 (2009).
[25] M. Cardona and G. Güntherodt, Light Scattering in Solids II: Basic Concepts and Instrumentation (Springer-Verlag, Berlin, Heidelberg, New York, 1982).
[26] S. Buchanan, E. C. L. Ru, and P. G. Etchegoin, Phys. Chem. Chem. Phys. **11**, 7406 (2009).
[27] W. Zhang et al., J. Phys. Chem. C **111**, 1733 (2007).
[28] K. B. Biggs et al., J. Chem. Phys. **113**, 4581 (2009).
[29] R. L. Aggarwal et al., J. Raman Spectrosc. **40**, 1331 (2009).